JOURNAL OF GEOPHYSICAL RESEARCH, VOL. 115, A04216, doi:10.1029/2009JA014836, 2010

Self-consistent ionospheric plasma density modifications by field-aligned currents: Steady state solutions

A. J. B. Russell,[1] A. N. Wright,[1] and A. W. Hood[1]

Received 25 August 2009; revised 19 November 2009; accepted 25 November 2009; published 27 April 2010.

[1] The magnetosphere and ionosphere are coupled by field-aligned currents that remove or deposit E-region electrons. Changes in electron number density modify ionospheric reflectivity, hence altering the magnetospheric current. Thus, self-consistent solutions are nontrivial. In this paper, we present 1-D steady states that self-consistently model modifications of ionospheric plasma density by field-aligned currents. These are used to investigate the width broadening and minimum plasma density of E-region plasma density cavities and the origin of small-scale features observed in downward current channels. A plasma density cavity forms and broadens if the maximum initial current density $j_{\|0}$ exceeds $j_c = \alpha n_e^2 he/(1 + 1/\beta)$, where α is the recombination coefficient, n_e is the equilibrium E-region number density in the absence of currents, h is the E-region thickness, and $\beta = \Sigma_{P0}/\Sigma_A$ is the initial ratio of Pedersen to magnetospheric Alfvén conductivities. If a plasma density cavity forms, its final width increases monotonically with $\mathcal{W} = 2B_0/\mu_0 V_A \alpha n_e^2 he$, where B_0 is the background magnetic field strength and V_A is the magnetospheric Alfvén speed. The minimum E-region number density, and the finest length scale present in the steady state, both scale as $1/\beta$. For typical ionospheric parameters and $j_{\|0} = 5\ \mu\mathrm{Am}^{-2}$, the fine scale is comparable to or less than $6\lambda_e$ for $\beta \gtrsim 2$, where λ_e is the electron inertial length. This suggests that electron inertial effects may become significant and introduce small-scale features, following the production of a single fine scale by depletion and broadening.

Citation: Russell, A. J. B., A. N. Wright, and A. W. Hood (2010), Self-consistent ionospheric plasma density modifications by field-aligned currents: Steady state solutions, *J. Geophys. Res.*, *115*, A04216, doi:10.1029/2009JA014836.

1. Introduction

[2] Wherever field-aligned currents close through the ionosphere, the magnetosphere and ionosphere form a strongly coupled system. This occurs, for example, in the auroral regions, where the upward current responsible for the northern lights is accompanied by a downward return current.

[3] A current system influences the ionosphere by modification of E-region electron number density. Upward currents enhance electron number densities by depositing electrons (which may then produce further ionization), while downward currents suppress them by removing electrons. The currents close through the ionosphere via Pedersen currents, as ions move horizontally to preserve quasi-neutrality. Typical current densities are readily sustained in the upward current channel, since the magnetosphere provides a large reservoir of electrons [*Wright et al.*, 2002; *Wright*, 2005]. In contrast, downward currents can rapidly suppress the ionospheric number density (on a time scale of ~30 s) and can lead to the formation of a plasma density cavity in the E-region [*Doe et al.*, 1995; *Blixt and Brekke*, 1996; *Karlsson and Marklund*, 1999; *Marklund et al.*, 2001; *Aikio et al.*, 2002, 2004].

[4] The depletion of ionospheric densities means that the downward current cannot maintain a large current density. The downward current channel (and region of suppressed number density) therefore has to broaden. This ensures that the total downward current remains the same, closing the current system, but is produced over a larger area, requiring lower current densities [*Marklund et al.*, 2001; *Aikio et al.*, 2002, 2004; *Cran-McGreehin et al.*, 2007].

[5] Fine scales present in the steady state are of great importance. Because of coupling of the ionosphere and magnetosphere, rapid variation in ionospheric number density produces small-scale current features in the magnetosphere. It is now well established that small-scale currents and electric fields are frequently observed in downward current channels [*Paschmann et al.*, 2002; *Mishin et al.*, 2003; *Wright et al.*, 2008]. Physical mechanisms that produce fine-scale features include the ionospheric feedback instability (IFI) or generalization of Ohm's Law to include electron inertia [*Streltsov and Lotko*, 2004, 2008].

[6] In this paper, we present steady state solutions for a 1-D model of a coupled magnetosphere-ionosphere system.

[1] School of Mathematics and Statistics, University of St. Andrews, North Haugh, St. Andrews, UK.

0148-0227/10/2009JA014836

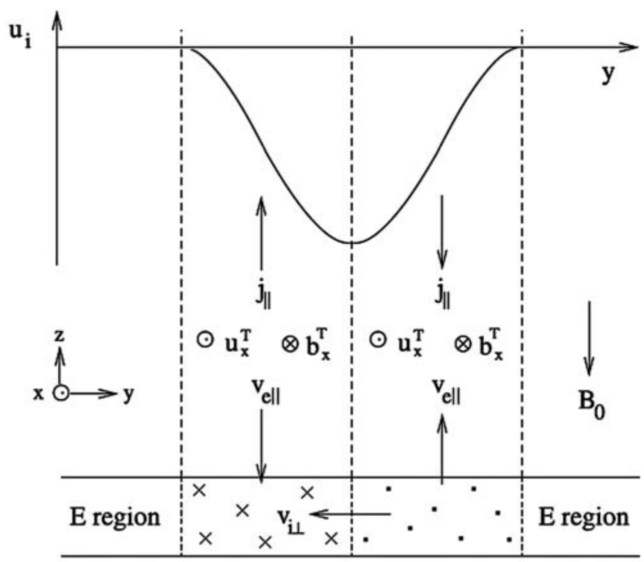

Figure 1. Diagram of the y-z plane of the model. An Alfvén wave, incident on the ionosphere, leads to the shearing of field lines, producing a channel of upward field-aligned current and a channel of downward field-aligned current. Upward field-aligned current deposits electrons into the ionosphere, enhancing number densities there (region marked with crosses). Downward field-aligned current removes electrons from the ionosphere, leading to electron depletion (region marked with dots).

We show that an analytic solution can be constructed for any field-aligned current system driven by an incident Alfvén wave. Having obtained this steady state, we also find a condition for formation of a plasma density cavity and broadening of the downward current channel, the minimum density, width of the plasma density cavity, and a guide to the finest length scale present in the steady state.

2. Model

[7] We employ the model described by *Cran-McGreehin et al.* [2007]. This uses a Cartesian coordinate system in which the background magnetic field, directed downward in the Northern Hemisphere, points in the negative z direction. A thin "sheet" ionosphere (representing the E-region) is located between $z = 0$ and $z = h$, and underlies a magnetosphere of uniform number density. Fields are considered invariant in the x direction. A diagram of the yz plane summarizes the model and is provided as Figure 1.

[8] Field-aligned currents are modeled by specifying an incident magnetospheric Alfvén wave, originating at $z = \infty$. This propagates downward, meeting the top of the ionosphere at $t = 0$, defining the time origin. At later times, the incident wave induces Pedersen currents in the ionosphere, leading to partial reflection of the incident wave.

[9] The incident velocity perturbation $-u_i(y)\hat{\mathbf{x}}$ is polarized in the x direction, producing a magnetic field perturbation $b_i(y)\hat{\mathbf{x}}$ by advection of field lines. Hence, gradients in $u_i(y)$ lead to gradients in $b_i(y)$, resulting in an incident field-aligned current.

[10] In order to consider localized physical solutions, we specify an incident velocity perturbation for which u_i and du_i/dy go to zero as $y \to \pm\infty$. This is equivalent to zero transverse electric field and zero field-aligned current at $y = \pm\infty$, forcing currents to close locally. It follows that there is at least one channel of upward current and one channel of downward current incident on the ionosphere. Ionospheric Pedersen current closes the magnetospheric current by flowing from the downward current region to the upward current region.

[11] At $t = 0$, the ionosphere is in an equilibrium state in which losses due to recombination are exactly balanced by gains from ionization. As yet, no electrons have been deposited or removed by currents. At later times, upward/downward field-aligned currents act as additional gain/loss terms in the ionospheric electron continuity equation, leading to enhanced/suppressed ionospheric number densities. The steady state is obtained once a new balance is reached between ionization, recombination, and field-aligned currents.

[12] For any physical scenario, one can define a length scale over which the magnetospheric density, magnetic field strength, and wavefields vary significantly. If this is much larger than the ionospheric thickness h, then the model which we have described can be applied. The remaining assumption, that of vertical background magnetic field, is reasonable for high latitudes.

3. Governing Equation

[13] Following the approach of *Streltsov and Lotko* [2005] and *Cran-McGreehin et al.* [2007], we begin with the continuity equation for electrons in the E-region of the ionosphere:

$$\frac{\partial n}{\partial t} = \frac{1}{e}\frac{\partial j_z}{\partial z} + \alpha\left(n_e^2 - n^2\right). \tag{1}$$

Here n is the electron number density, j_z is the vertical current, e is the fundamental charge, n_e is the equilibrium electron density in the absence of field-aligned currents, and α is the recombination coefficient which we take to be constant.

[14] Equation (1) can be integrated over the thickness of the E-region. If n is independent of height, then the height-integrated electron density is $N = hn$, where h is the thickness of the E-region. Also, $j_z = 0$ at the base of the E-region. Thus, integration of (1) gives

$$\frac{\partial N}{\partial t} - \frac{j_z}{e} = \frac{\alpha}{h}\left(N_e^2 - N^2\right), \tag{2}$$

where j_z now represents the current at the top of the E-region.

[15] Positive vertical currents are directed upward, and are carried by a downward flow of electrons. Therefore, these currents deposit electrons in the E-region and act as a gain term in the continuity equation. Similarly, negative currents act as a loss term. The term $\alpha N_e^2/h$ is a source term representing ionization and $-\alpha N^2/h$ is a loss term representing recombination. In the absence of field-aligned currents, the steady state is satisfied by $N = N_e$.

[16] Field-aligned currents are driven by an incident Alfvén wave that is reflected by the ionosphere. Writing $b_i(y)\hat{\mathbf{x}}$ and $-u_i(y)\hat{\mathbf{x}}$ as the incident wave magnetic and velocity perturbations, the total magnetospheric perturbations are given by

$$u_x^T(y) = (1+r)u_i \tag{3}$$

$$b_x^T(y) = (1-r)b_i, \tag{4}$$

where

$$r = \frac{1-\mu_0\Sigma_P V_A}{1+\mu_0\Sigma_P V_A} \tag{5}$$

and

$$b_i = \frac{B_0 u_i}{V_A}. \tag{6}$$

The variable r is the reflection coefficient for the ionosphere, assuming that the current closes in the E-region, resulting in the atmosphere being shielded from the magnetospheric magnetic perturbation b_x^T. $\Sigma_P = \Sigma_{P0}N/N_e$ represents the height-integrated Pedersen conductivity, B_0 is the background magnetic field strength, ρ_0 is the magnetospheric ion density, and $V_A = B_0/\sqrt{\mu_0\rho_0}$ is the magnetospheric Alfvén speed.

[17] Substituting (5) and (6) into (4) and differentiating to obtain

$$j_z = -\frac{1}{\mu_0}\frac{\partial b_x^T}{\partial y}, \tag{7}$$

the height-integrated continuity equation (2) may be written as

$$\frac{\partial}{\partial t}\left(\frac{N}{N_e}\right) + \frac{\partial}{\partial y}\left(\frac{\eta u_i N}{N_e+\beta N}\right) = \kappa\left(1-\frac{N^2}{N_e^2}\right), \tag{8}$$

where

$$\kappa = \frac{\alpha N_e}{h}, \tag{9}$$

$$\eta = \frac{2\Sigma_{P0}B_0}{N_e e}, \tag{10}$$

and

$$\beta = \mu_0 V_A \Sigma_{P0} \equiv \frac{\Sigma_{P0}}{\Sigma_A}. \tag{11}$$

Here N is the primary dependent variable of our system, from which magnetospheric perturbations, ionospheric currents, and field-aligned currents may be directly obtained, given knowledge of u_i and equilibrium quantities. Also, β represents the ratio of the Pedersen conductivity to the Alfvén conductivity, $\Sigma_A = 1/\mu_0 V_A$, in the absence of field-aligned current. It will be seen to be an important descriptor of the system.

[18] In the steady state, (8) reduces to

$$\frac{d}{dy}\left(\frac{\eta u_i N}{N_e+\beta N}\right) = \kappa\left(1-\frac{N^2}{N_e^2}\right), \tag{12}$$

which is the focus of this paper.

4. Numerical Solution

4.1. Method

[19] To obtain example solutions to the steady state equation (12), we used a numerical scheme to evolve an initial state

$$N = N_e \quad \text{at} \quad t = 0, \tag{13}$$

according to the time-dependent governing equation (8). Numerically, it is convenient to solve this in a normalized form, putting

$$\bar{y} = \frac{y}{y_0}, \tag{14}$$

$$\bar{u}_i = \frac{u_i}{u_{i0}}, \tag{15}$$

$$\bar{t} = \frac{t}{\tau} = \frac{u_{i0}t}{y_0}, \tag{16}$$

$$\bar{N} = \frac{N}{N_e}, \tag{17}$$

$$\bar{\kappa} = \tau\kappa = \frac{y_0\kappa}{u_{i0}}, \tag{18}$$

where y_0, u_{i_0}, and τ are the characteristic length scale, incident velocity, and time scale, respectively. This means that a numerical steady state represents a family of steady states, since it can be scaled by y_0 and u_{i_0}.

[20] The code uses an Euler scheme and evaluates spatial derivatives as forward differences. This results in a code that is first order in both time and space and that can evolve discontinuities in number density. The high spatial resolution required to resolve fine scales means that a higher order scheme would not significantly improve accuracy. For the runs presented here, the spatial resolution is $\delta\bar{y} = 0.001$ and the time resolution is $\delta\bar{t} = 0.0001$. The parameters $\eta = 1.015$, $\alpha = 3\times10^{-13}$ m^3 s^{-1}, $h = 2\times10^4$ m, and $N_e = 1.2\times10^{15}$ m^{-3} were fixed across all runs, while β was varied between them.

[21] The velocity profile was taken as

$$\bar{u}_i = \begin{cases} -(1+\cos(\bar{y})), & \text{for } -\pi < \bar{y} < \pi \\ 0 & \text{otherwise,} \end{cases} \tag{19}$$

producing an incident current that is upward between $-\pi$ and 0, downward between 0 and π, and zero everywhere else. We chose to keep the maximum initial current density in the downward channel constant across all simulations, using a

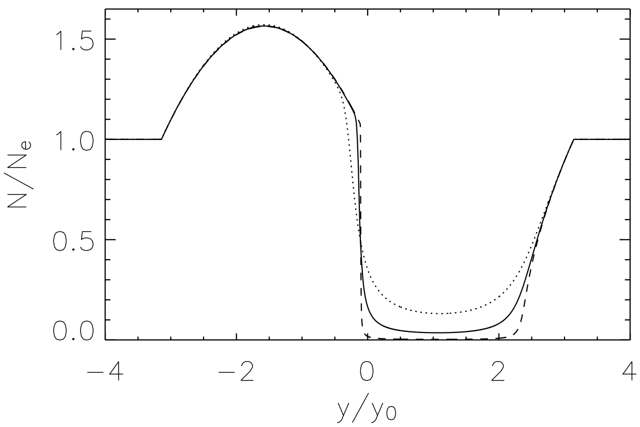

Figure 2. Numerical steady states for $\beta = 20$ (dotted curve), $\beta = 100$ (solid curve), and $\beta = 1370$ (dashed curve). As β is increased, the suppression of number densities in the downward current channel becomes more severe. The finest scale present in each steady state is seen to decrease with increasing β, leading to steeper gradients.

value of $j_{\|0} = 5 \times 10^{-6}$ μAm^{-2}. This includes a contribution from the reflected wave and is enforced by the condition

$$\tau = \frac{y_0}{u_{i0}} = \frac{2B_0\Sigma_{P0}}{(1+\beta)j_{\|0}}. \tag{20}$$

[22] Since $\overline{u}_i = 0$ at the edges of the simulation domain, the governing equations provide tests for the simulations. If $\alpha = 0$, then (8) conserves the integrated number density. To test the code, a run was performed with $\alpha = 0$ and $\beta = 100$ (all other parameters were set as stated above). During this run, the dimensionless integrated number density varied from its initial value of 8.0 by less than 1.78×10^{-14}.

[23] Taking $\alpha \neq 0$, (12) implies that the integral of $(1 - \overline{N}^2)$ over the simulation domain is zero in the steady state. The physical interpretation of this is that ionization and recombination balance one another in the steady state. Evaluating the integral allows us to check convergence to the steady state: all the steady states referred to in this paper were obtained by running simulations until $|\int(1 - \overline{N}^2)d\overline{y}|$ was less than 1.0×10^{-10} and slowly converging to zero, as evaluated over the simulation domain.

4.2. Results

[24] Figure 2 shows steady states for $\beta = 12.2$, 100, and 1370. In the upward current channel, the ionospheric number density is enhanced, the solution varying little with β. In the downward current channel, number densities are suppressed to a degree that increases with β.

[25] The finest length scale present in each steady state is located at the boundary between the upward and downward current channels. Here the number density changes rapidly over a distance that decreases with increasing β. We investigated the relationship between fine scales and β by determining the steepest gradient in each steady state from finite differencing. Plotting this gradient against β, as in

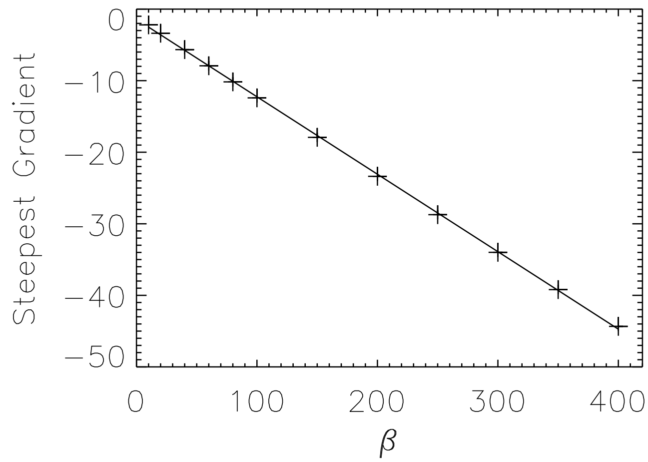

Figure 3. Demonstration that the steepest gradient in the numerical steady state is linear in β. Points represent simulations and the straight line is a best fit to the data, given by -1.42–0.108β. This linear relationship implies that the finest length scale present in the steady state goes as $1/\beta$.

Figure 3, reveals that the steepest gradient varies linearly with β. The best fit straight line is -1.42–0.108β, giving

$$\lambda \approx \frac{9.24y_0}{\beta} \tag{21}$$

as the fine scale for runs in which $\beta \gg 13$.

[26] Defining $N_{\min}$ as the minimum value of N in the steady state, it is seen that $N_e/N_{\min}$ is linear in β for the numerical solutions (Figure 4). The best fit straight line is $2.64 + 0.253\beta$, implying that

$$N_{\min} \approx \frac{3.95N_e}{\beta} \tag{22}$$

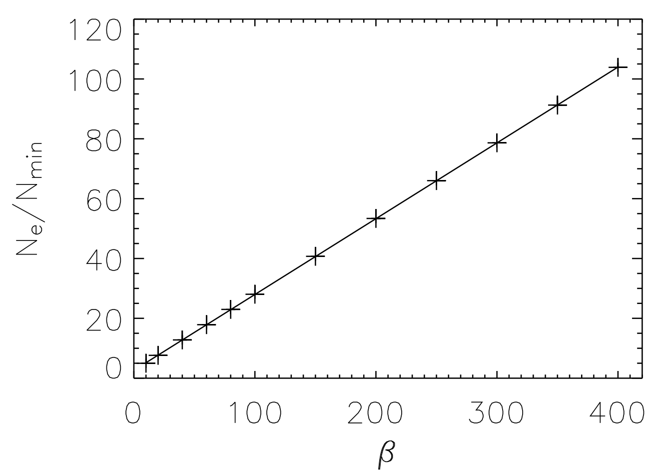

Figure 4. Demonstration that $N_e/N_{\min}$ is linear in β for the numerical steady states. Points represent simulations and the straight line is a best fit to the data, given by $2.64 + 0.253\beta$. This linear relationship implies that $N_{\min}$ goes as $1/\beta$.

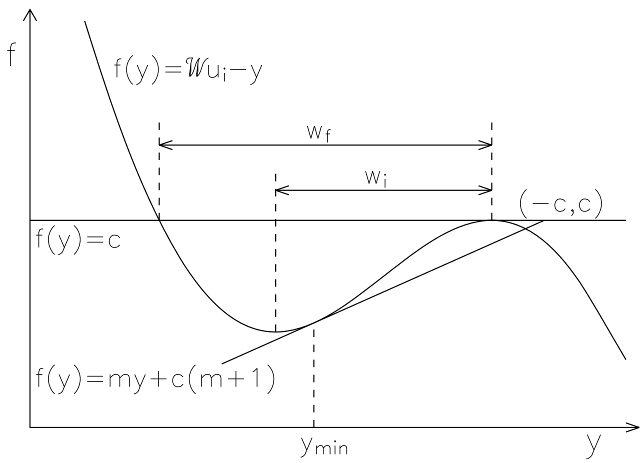

Figure 5. Sketch of $\mathcal{W}u_i$-y against y, from which many key features of the solution can be determined. The horizontal line, passing though the maximum turning point determines the integration constant c. The horizontal distance between the turning points w_i indicates the initial width with which the plasma density cavity forms. The distance between the intersections $\mathcal{W}u_i$-y = c, w_f, indicates the final width of the plasma density cavity. A straight line may be drawn through the point ($-c$,c) that is tangent to $\mathcal{W}u_i - y$ between its turning points. The tangent meets the curve at the location of the minimum in number density $y_{\min}$, and the minimum number density is $N_e/\beta m$, where m is the slope of the tangent.

for $\beta \gg 10$. Introducing $y_{\min}$ as the position of the minimum, $1/(\mathcal{W}u'(y_{\min}) - 1) = 3.86$ for $\beta = 400$. Hence, the constant of proportionality in (22) is in good agreement with the analytic result, equation (32).

5. Analytic Solution

[27] The steady state equation (12) may be solved directly in two limits. The first of these assumes that $\beta N \gg N_e$, and is valid where depletion has not significantly altered the reflection coefficient from $r = -1$ (the ionosphere remains highly reflective). This leads to an upper steady state solution N_{upper}. The second assumption is to take $N^2 \ll N_e^2$. This corresponds to significant depletion, so that recombination is negligible, leading to a lower solution N_{lower}. Once these have been obtained, the global solution can be constructed through boundary layer matching.

5.1. Upper Solution

[28] Where $\beta N \gg N_e$, (12) reduces to

$$\frac{\eta}{\beta}\frac{du_i}{dy} = \kappa\left(1 - \frac{N^2}{N_e^2}\right). \tag{23}$$

We can rearrange this directly to obtain the upper steady state solution

$$N_{\text{upper}} = N_e\sqrt{1 - \frac{\eta}{\kappa\beta}\frac{du_i}{dy}}. \tag{24}$$

Note the role of the parameter

$$\mathcal{W} = \frac{\eta}{\kappa\beta} = \frac{2B_0}{\alpha h n_e^2 e\mu_0 V_A} \tag{25}$$

that has the dimension of time. (This appears in *Cran-McGreehin et al.* [2007] in its dimensionless form, normalized by τ.) If $\mathcal{W}du_i/dy \leq 1$ then N_{upper} is real; otherwise, N_{upper} is imaginary. This means that the upper solution breaks down at points where

$$\mathcal{W}\frac{du_i}{dy} = 1, \tag{26}$$

If $\max(\mathcal{W}du_i/dy) > 1$, then a lower solution is required.

5.2. Lower Solution

[29] Where $N^2 \ll N_e^2$, (12) reduces to

$$\frac{d}{dy}\left(\frac{\eta u_i N}{N_e + \beta N}\right) = \kappa. \tag{27}$$

Integrating this directly and rearranging yields the lower steady state solution

$$N_{\text{lower}} = \frac{N_e\kappa(y+c)}{\eta u_i - \kappa\beta(y+c)}, \tag{28}$$

where c is an integration constant.

[30] The lower solution breaks down at points where the denominator goes to zero. This occurs for

$$c = \mathcal{W}u_i(y) - y. \tag{29}$$

It follows that c can be determined if there is a known location at which the lower solution must break down.

[31] Broadening is seen to occur on the side of the downward current region at which the Pedersen current j_P has the same sign as the spatial gradient of number density $\partial N/\partial y$. Since we require that Pedersen currents close the field-aligned currents locally, this means that the depleted trough broadens on the side adjacent to the upward current region.

[32] A complete steady state that has broadened on one side, can be constructed, if, and only if, upper and lower solutions break down at common point, on the side of the trough that has not broadened. The best way to visualize this is to examine a plot of $\mathcal{W}u_i - y$, an illustration of which is given in Figure 5. By (26), the upper solution breaks down at the turning points of this curve; by (29), the lower solution breaks down at intersections with $\mathcal{W}u_i - y = c$. Hence, the condition that the steady state follows broadening on one side requires $f(y) = c$ to intersect the turning point of $f(y) = \mathcal{W}u_i - y$ farthest from the upward current region (always a maximum). Therefore, the value of the integration constant c is readily determined, providing a unique lower solution.

5.3. Minimum E-Region Plasma Density

[33] If $\mathcal{W}du_i/dy < 1$ everywhere, then the upper solution gives a complete description of the steady state. In such a

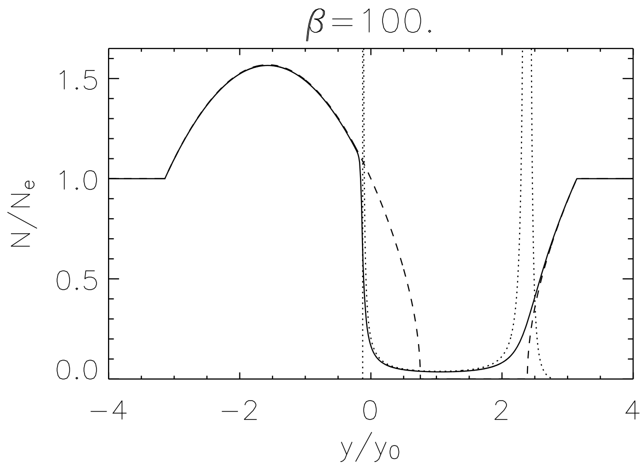

Figure 6. Plot showing the steady state obtained numerically for β = 100 (solid line) with the upper steady state (dashed curve) and lower steady state (dotted curve).

case, the minimum E-region plasma density is located where the initial current density is at its maximum, and

$$N_{\min} = N_e \sqrt{1 - \max\left(\mathcal{W}\frac{du_i}{dy}\right)}. \tag{30}$$

[34] If max($\mathcal{W}du_i/dy$) > 1, then the density minimum is obtained from the lower solution. Writing $y_{\min}$ as the location of the density minimum, $y_{\min}$ satisfies

$$u_i(y_{\min}) - u_i'(y_{\min})(y_{\min} + c) = 0 \tag{31}$$

and the minimum density is

$$N_{\min} = \frac{N_e}{\beta(\mathcal{W}u_i'(y_{\min}) - 1)}. \tag{32}$$

In practice, $\mathcal{W}u_i'(y_{\min})$ is weakly dependent on β, remaining of order ~1. Hence, the main dependence on β is $N_{\min} \sim 1/\beta$, in keeping with the numerical results presented in section 4.2.

[35] When the lower solution exists, the location and value of the density minimum may be obtained from a plot of $\mathcal{W}u_i - y$ against y (Figure 5). At $y_{\min}$, the curve has gradient $m = \mathcal{W}u_i'(y_{\min}) - 1$. Therefore, multiplying (31) through by $\mathcal{W}$, putting $\mathcal{W}u_i'(y_{\min}) = m + 1$, and rearranging for m, we may write

$$m = \frac{c - (\mathcal{W}u_i(y_{\min}) - y_{\min})}{(-c) - y_{\min}}. \tag{33}$$

Hence, a straight line through the point ($-c$, c) that is tangent to $\mathcal{W}u_i - y$ between its turning points must meet the curve at $y_{\min}$. Furthermore, (32) allows us to write

$$N_{\min} = \frac{N_e}{\beta m}, \tag{34}$$

where m is the slope of the tangent.

5.4. Plasma Density Cavity: Formation, Width, and Broadening

[36] If max($\mathcal{W}du_i/dy$) < 1, then the upper solution gives a complete description of the steady state, and the reflection coefficient is not significantly altered from $r = -1$. In such a case, density is suppressed, but a true plasma density cavity does not form.

[37] If max($\mathcal{W}du_i/dy$) > 1, then a plasma density cavity is present in the steady state. We may discuss both an initial width, with which the plasma density cavity first forms, and a final width, which it attains by broadening.

[38] The initial width may be estimated as the distance between the two points at which the upper solution breaks down. These are the points at which $\mathcal{W}u_i'(y) = 1$. Inspection of a plot of $\mathcal{W}u_i - y$ against y (Figure 5) yields this as the horizontal distance between the two turning points (marked as w_i).

[39] Similarly, the final width may be estimated as the distance between the two points at which the lower solution breaks down. These are the points at which $\mathcal{W}u_i - y = c$. Referring to the plot of $\mathcal{W}u_i - y$ against y (Figure 5), this final width is the horizontal distance between intersections of $f(y) = \mathcal{W}u_i - y$ and $f(y) = c$ (marked as w_f). It can be seen that, regardless of the value of c, the final width increases monotonically with $\mathcal{W}$. Writing $y = a$ and $y = b$ for the limits of the plasma density cavity, where $b > a$, the final width satisfies

$$w_f = b - a = \mathcal{W}(u_i(b) - u_i(a)). \tag{35}$$

The strong dependence on $\mathcal{W}$ is apparent. Recalling that $u_i \to 0$ at the edge of the current system, it is also clear that the plasma density cavity cannot expand beyond the limits of the current system.

[40] Since the minimum turning point of $f(y) = \mathcal{W}u_i - y$ lies between the intersections with $f(y) = c$, the final width of the plasma density cavity is always greater than the initial width. If max($\mathcal{W}du_i/dy$) < 1, then $\mathcal{W}u_i - y$ does not possess turning points. This means that it is not possible to discuss the width of a plasma density cavity in the same way as for max($\mathcal{W}du_i/dy$) > 1. It follows that the condition max ($\mathcal{W}du_i/dy$) > 1 is a robust condition for the formation and broadening of a plasma density cavity (and hence broadening of the downward current channel).

5.5. Global Solution by Boundary Layer Matching

[41] Once upper and lower steady states have been determined, the global steady state can be accurately approximated using a boundary layer analysis. The principle is that we can use the upper steady state where there is little depletion and the lower steady state where depletion is significant. There are, however, two narrow regions in which neither approximation is valid, and the solution makes a transition between the upper and lower steady states (Figure 6). We solve the full steady state equation in each of these regions, but simplify matters by assuming regions are narrow and a solution need only be valid within the appropriate boundary region. Once we have boundary layer solutions, the global steady state can be constructed.

[42] Here we outline the method and results of this analysis, reserving detailed working for the appendices. For a

boundary layer positioned at $y = \xi$ (a location at which the lower solution breaks down), the method is as follows:

[43] 1. Introduce a scaling of the form

$$Y = \beta^{\epsilon}(y - \xi) \quad (36)$$

$$\mathcal{N} = \beta^{\nu} N / N_e, \quad (37)$$

where $\epsilon > 0$. This provides a stretched coordinate Y that is small within the boundary layer.

[44] 2. Expand $\mathcal{N}^2_{\text{upper}}(Y)$ and $\mathcal{N}_{\text{lower}}(Y)$ about ξ. Since u_i is regular at ξ, it has a Taylor expansion

$$u_i(Y) = u_i(\xi) + u_i'(\xi)\beta^{-\epsilon}Y + \frac{u_i''(\xi)}{2}\beta^{-2\epsilon}Y^2 + \ldots, \quad (38)$$

where a prime denotes differentiation with respect to y.The expression $\mathcal{N}_{\text{upper}}(Y)$ is readily obtained from $\mathcal{N}^2_{\text{upper}}(Y)$, and inspection reveals the behavior of the upper and lower solutions as $Y \to 0$. At this stage, ϵ and ν may be fixed as described in Appendix A.

[45] 3. Expand $\mathcal{N}$. Led by the occurrence of powers of $\beta^{-\epsilon}$ in the expansion of u_i, we expand $\mathcal{N}$ as

$$\mathcal{N} = \mathcal{N}_0 + \mathcal{N}_1\beta^{-\epsilon} + \mathcal{N}_2\beta^{-2\epsilon} + \ldots. \quad (39)$$

If $\beta^{-\epsilon} < 1$, then $\mathcal{N}_0$ is an approximation for $\mathcal{N}$, while $\mathcal{N}_1$, etc., provide corrections. The smaller the value of $\beta^{-\epsilon}$, the better the approximation.

[46] 4. Substitute expansions of $\mathcal{N}^2_{\text{upper}}$, u_i, and $\mathcal{N}$ into the scaled governing equation; equate terms in β^0. This gives an ordinary differential equation for $\mathcal{N}_0$. Solutions for $\mathcal{N}_1$ and higher order corrections may be obtained by equating lower powers of β in the scaled governing equation.

[47] 5. Construct the global solution across the boundary layer. Let $\mathcal{N}_{\text{outer}}$ be the steady state solution (either $\mathcal{N}_{\text{upper}}$ or $\mathcal{N}_{\text{lower}}$) that is valid to the left of the boundary layer. We introduce $g(Y)$ as the leading order behavior of $\mathcal{N}_{\text{outer}}$ as $Y \to 0$, making sure that $g(Y)$ includes all singular terms. We also put

$$\mathcal{N}_{\text{inner}} = \mathcal{N}_0 + \ldots + \mathcal{N}_{r-1}\beta^{-(r-1)\epsilon}, \quad (40)$$

where $r \in \mathbb{N}$ matches or exceeds the number of singular terms in $\mathcal{N}_{\text{outer}}$. The complete solution can be constructed on the left of the boundary layer, provided $\mathcal{N}_{\text{inner}} \to g(Y)$ as $Y \to -\infty$. That is to say, the behavior of the inner solution as $Y \to -\infty$ matches the behavior of the outer solution as $Y \to 0$. (This is true for solutions constructed in this paper.) The solution to the left of ξ is

$$\mathcal{N} \approx \mathcal{N}_{\text{inner}} + \mathcal{N}_{\text{outer}} - g(Y). \quad (41)$$

A similar construction applies to the right of ξ.

[48] 6. Rewrite the complete solution in terms of the original, unscaled variables N and y.

[49] Between the upward and downward current channels, the scaling is $\epsilon = 1$, $\nu = 0$. Farthest from the upward current channel, the scaling is $\epsilon = 2/5$, $v = 1/5$. Equation (36) informs us that the width of each boundary layer scales as $\beta^{-\epsilon}$. It follows that the finest length scale in our steady state goes as $1/\beta$, and that this occurs between the upward and downward channels. This agrees with the numerical simulations presented in section 4 (Figure 3).

[50] Matching between the upward and downward current channels, the unscaled solution is

$$N = N_0 + N_{\text{upper}} - N_s \quad (42)$$

on the upper steady state side of ξ and

$$N = N_0 + N_{\text{lower}} + \frac{N_e^3 \mathcal{W} u_i(\xi)}{\beta N_s^2 (y - \xi)} \quad (43)$$

on the lower steady state side of ξ, where

$$N_s = N_{\text{upper}}(\xi), \quad (44)$$

and N_0 is given implicitly by

$$-\frac{\beta(y-\xi)}{N_e^3 W u_i(\xi)} = \frac{1}{N_s^2 N_0} + \frac{1}{2N_s^3}\ln(N_s - N_0) - \frac{1}{2N_s^3}\ln(N_s + N_0). \quad (45)$$

[51] For the boundary layer farthest from the upward current channel, the unscaled solution is

$$N = N_0 + \beta^{-2/5}N_1 + N_{\text{upper}} - N_e\sqrt{-\mathcal{W}u_i''(\xi)(y-\xi)} + \frac{N_e u_i'''(\xi)\sqrt{-\mathcal{W}u_i''(\xi)(y-\xi)}(y-\xi)}{4u_i''(\xi)}, \quad (46)$$

on the upper steady state side of ξ and

$$N = N_0 + \beta^{-2/5}N_1 + N_{\text{lower}} - \frac{2N_e u_i(\xi)\beta^{-1}}{u_i''(\xi)(y-\xi)^2} + \left(\frac{2u_i'(\xi)}{u_i''(\xi)} - \frac{2u_i(\xi)u_i'''(\xi)}{3u_i''(\xi)}\right)\frac{N_e\beta^{-1}}{(y-\xi)} \quad (47)$$

on the lower steady state side of ξ, where N_0 and N_1 are the solutions of the following ordinary differential equations:

$$\frac{dN_0}{dy} = -\frac{\beta N_0}{\mathcal{W}u_i(\xi)} + \frac{\beta u_i''(\xi)}{N_e u_i(\xi)}N_0^2(y-\xi) \quad (48)$$

$$\frac{dN_1}{dy} = \frac{N_0}{\mathcal{W}u_i(\xi)}\left(\beta^{2/5} - \frac{\beta N_0^2 N_1}{N_e^3}\right) + \frac{N_0}{N_e u_i(\xi)}\left(\frac{\beta^{7/5}N_0^3}{N_e^2\mathcal{W}^2 u_i(\xi)} - 2\beta N_1 u_i''(\xi)\right)(y-\xi) + \frac{\beta^{7/5}N_0^2}{N_e u_i(\xi)}\left(\frac{u_i''(\xi)}{\mathcal{W}u_i(\xi)} - \frac{u_i'''(\xi)}{2}\right)(y-\xi)^2. \quad (49)$$

These can be solved numerically if we note that the asymptotic behavior

$$N_0 \approx -N_e\sqrt{\mathcal{W}u_i''(\xi)(y-\xi)} \quad (50)$$

$$N_1 \approx -\frac{N_e\beta^{2/5}u_i'''(\xi)\sqrt{\mathcal{W}u_i''(\xi)(y-\xi)}(y-\xi)}{4u_i''(\xi)}, \quad (51)$$

as $|y| \to \infty$ in the direction of the upper steady state (see Appendix C), provides boundary conditions for numerical integration.

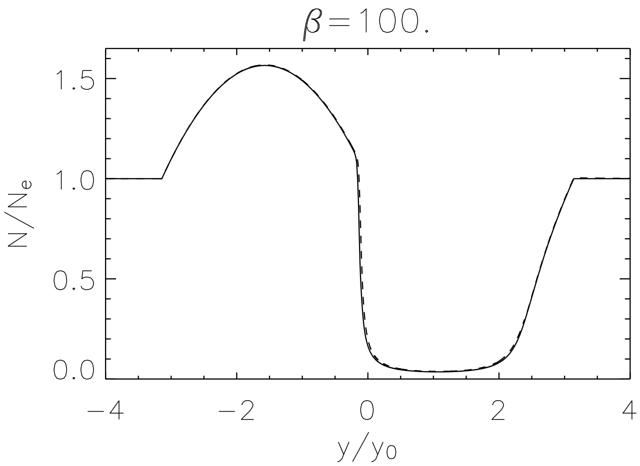

Figure 7. Comparison of steady states obtained numerically (solid line) and analytically (dashed line) for $\beta = 100$.

[52] If the boundary matching between the upward and downward channels is performed at $y = a$, and the matching far from the upward channel is performed at $y = b$, then the complete solution can be constructed by using (42) and (46) out with the plasma density cavity, and taking

$$N = N_{\text{lower}} + N_{a0} + N_{b0} + \beta^{-2/5}N_{b1} + \frac{N_e^3 \mathcal{W} u_i(a)}{\beta N_s^2(y-a)} - \frac{2N_e u_i(b)\beta^{-1}}{u_i''(b)(y-b)^2} + \left(\frac{2u_i'(b)}{u_i''(b)} - \frac{2u_i(b)u_i'''(b)}{3u_i''(b)}\right)\frac{N_e\beta^{-1}}{(y-b)} \quad (52)$$

inside the plasma density cavity, where N_{a_0} is the solution to (45) with $\xi = a$, N_{b_0} is the solution to (48) with $\xi = b$, and N_{b_1} is the solution to (49) with $\xi = b$.

[53] We test the analytic solution by comparison with numerical solutions. Figure 7 shows this comparison for $\beta = 100$. The agreement is excellent. For all numerical solutions with $\beta \geq 20$, the area between the two curves is less than 3.7% of the area under the numerical solution, with the best agreement obtained for large β. For very low values of β, agreement can be improved by including higher order corrections in the analytic solution.

6. Discussion and Conclusions

[54] We have obtained self-consistent steady states for ionospheric density modifications by field-aligned currents. These illustrate the large-scale features of such a system at late times, which may follow the formation and broadening of an ionospheric plasma density cavity. The method is applicable to any current system driven by an incident Alfvén wave. In addition to detailing how to compute these steady states, we have investigated the formation and broadening of density cavities, their width, the minimum density, and the finest scale in the steady state.

[55] The steady state solutions have revealed that the downward current channel broadens for $\max(\mathcal{W} du_i/dy) > 1$ (section 5.1). Using (25) to evaluate $\mathcal{W}$, using (4)–(7) to evaluate du_i/dy, and writing $j_{\|0}$ for the greatest initial downward current density, this condition becomes

$$(1 + 1/\beta)\frac{j_{\|0}}{\alpha h n_e^2 e} > 1. \quad (53)$$

Hence, for given α, h, n_e and $\beta = \Sigma_{\text{P0}}/\Sigma_{\text{A}}$, there is a maximum current intensity j_c that can be supported without broadening. Rearranging (53)

$$j_c = \frac{1}{(1 + 1/\beta)}\alpha n_e^2 h e. \quad (54)$$

In the limit $\beta \gg 1$, (53) and (54) are independent of β, and reproduce equations (32) and (33) of *Cran-McGreehin et al.* [2007]. This represents a generalization of their result to any current system and for any value of β.

[56] Downward current density can be maintained over a region of ionosphere if and only if electrons can be produced at a sufficient rate. Examining (54), αn_e^2 is the ionization rate in the ionosphere. The maximum rate at which charge can be produced in the ionosphere is therefore $\alpha n_e^2 h e$. If the downward current density exceeds this, then the current can only be maintained if the current channel broadens, reducing the current density. The factor involving β represents the fact that broadening occurs for low β without completely evacuating the plasma density cavity of electrons and ions (the minimum electron number density goes as $1/\beta$). This means that recombination persists, so electrons produced by ionization must balance both current density and recombination. Therefore, the critical current is less than $\alpha n_e^2 h e$ for low β.

[57] We have demonstrated that the finest scale present in the steady state scales as $1/\beta$. Therefore, for given η, α, h, and N_e, there is always a threshold value of β above which additional terms should be included in Ohm's law. The Hall term can initially be neglected, since the linear order current is field-aligned, but electron inertia should be considered.

[58] The runs presented in section 4 exhibit a fine scale, $\lambda \approx 9.24 y_0/\beta$. The width of the simulated current channel is approximately $\pi\ y_0$ and compares with observations of ~25 km width after broadening [*Marklund et al.*, 2001]. Assuming a number density of $n_0 = 10^6$ in the magnetosphere gives an electron inertial length $\lambda_e = \sqrt{m_e/\mu_0 n_0 e^2}$ of 5.32 km. In a study of field line resonances, *Wei et al.* [1994] showed that electron inertial effects are important in the magnetosphere for $\lambda \lesssim 6\lambda_e$. Therefore, electron inertial effects should be considered of interest for $\beta \gtrsim 2$. This indicates that electron inertial effects may be present in the downward current channel, and might introduce small-scale features, following the production of a single fine-scale feature by depletion and broadening [*Streltsov and Lotko*, 2004; *Marklund et al.*, 2001; *Paschmann et al.*, 2002; *Mishin et al.*, 2003]. This promises a possible explanation for the origin of current filaments observed within downward current channels [*Wright et al.*, 2008].

Appendix A: Scalings

[59] In order to perform the boundary layer analysis, we use a stretched coordinate

$$Y = \beta^{\epsilon}(y - \xi), \quad (A1)$$

so that Y is small within the boundary layer. This is provided for $\epsilon > 0$. It may prove necessary to scale the density as well, so we write

$$\mathcal{N} = \beta^{\nu} N/N_e, \tag{A2}$$

noting that ν may be zero.

[60] We can rewrite the steady state equation (12) by applying the product and quotient rules to the derivative, noting that

$$\frac{N}{N_e + \beta N} = \frac{1}{\beta} - \frac{1}{\beta(1 + \beta N/N_e)}, \tag{A3}$$

and using (24). After rearranging, this yields

$$-\left(1 + \beta\frac{N}{N_e}\right)\frac{du_i}{dy} + u_i\beta\frac{d}{dy}\left(\frac{N}{N_e}\right) = \frac{1}{\mathcal{W}}\left(1 + \beta\frac{N}{N_e}\right)^2\left(\frac{N_{\text{upper}}^2}{N_e^2} - \frac{N^2}{N_e^2}\right). \tag{A4}$$

[61] Applying the scaling, this becomes

$$-\beta^{\epsilon+\nu-1}(\beta^{\nu-1} + \mathcal{N})\frac{du_i}{dY} + \beta^{\epsilon+\nu-1}u_i\frac{d\mathcal{N}}{dY} = \frac{\beta^{-2\nu}}{\mathcal{W}}\left(\beta^{\nu-1} + \mathcal{N}\right)^2 \cdot\left(\mathcal{N}_{\text{upper}}^2 - \mathcal{N}^2\right). \tag{A5}$$

[62] The parameters ϵ and ν are determined by inspecting (A5) and the expanded form of $\mathcal{N}_{\text{upper}}^2$. Assuming that the greatest power of β in an expansion of $\mathcal{N}$ is zero, and that $\nu < 1$, then matching terms in the leading order of β requires

$$\epsilon + 3\nu = 1, \tag{A6}$$

and that the greatest power of β in $\mathcal{N}_{\text{upper}}^2$ is zero.

[63] Between the upward and downward current channels, $\mathcal{N}_{\text{upper}}^2$ is nonsingular at ξ, so its leading order term is the constant $\mathcal{N}_{\text{upper}}^2(\xi)$. The greatest power of β is automatically zero, so we do not need to scale the density. Hence, we take

$$\nu = 0, \quad \epsilon = 1. \tag{A7}$$

[64] At the edge of the depleted region farthest from the upward current channel, $\mathcal{N}_{\text{upper}}^2$ is singular at ξ. Here the leading term is $\mathcal{W}u''_i(\xi)\beta^{2\nu-\epsilon}Y$, where primes denote differentiation with respect to y. Since we wish the greatest power of β to be zero, this gives

$$2\nu - \epsilon = 0. \tag{A8}$$

Solving this alongside (A6) yields

$$\nu = \frac{1}{5}, \quad \epsilon = \frac{2}{5}. \tag{A9}$$

[65] Alternatively, one may obtain scalings by inspection of $\mathcal{N}_{\text{upper}}$ and $\mathcal{N}_{\text{lower}}$, requiring that the greatest power of β be zero in each expansion. The same values are obtained for ϵ and ν.

Appendix B: Boundary Layer Matching Between Upward and Downward Current Channels

[66] First let us note that $\xi + c = \mathcal{W}u_i(\xi)$ and $N_s^2 = N_{\text{upper}}^2(\xi) = N_e^2(1 - \mathcal{W}u_i'(\xi)) > 0$, where primes denote differentiation with respect to y. These results are useful in what follows.

[67] We proceed according to the method outlined in section 5. Applying the scaling, and using (24), (28), and (38) to expand $\mathcal{N}_{\text{upper}}^2$ and $\mathcal{N}_{\text{lower}}$ about ξ gives

$$\mathcal{N}_{\text{upper}}^2 = \mathcal{N}_s^2 - \mathcal{W}u_i''(\xi)\beta^{2\nu-\epsilon}Y - \frac{\mathcal{W}u_i'''(\xi)\beta^{2\nu-2\epsilon}}{2}Y^2 - \ldots \tag{B1}$$

$$\mathcal{N}_{\text{lower}} = -\frac{\mathcal{W}u_i(\xi)\beta^{3\nu+\epsilon-1}}{\mathcal{N}_s^2 Y} - \frac{\beta^{3\nu-1}}{\mathcal{N}_s^2} - \frac{\mathcal{W}u_i''(\xi)\beta^{5\nu-1}}{2\mathcal{N}_s^4} - \ldots. \tag{B2}$$

[68] The scaling is determined as described in Appendix A, giving $\nu = 0$ and $\varepsilon = 1$. Thus, the above expansions become

$$\mathcal{N}_{\text{upper}}^2 = \mathcal{N}_s^2 - \frac{\mathcal{W}u_i''(\xi)}{\beta}Y - \frac{\mathcal{W}u_i'''(\xi)}{2\beta^2}Y^2 - \ldots \tag{B3}$$

$$\mathcal{N}_{\text{lower}} = -\frac{\mathcal{W}u_i(\xi)}{\mathcal{N}_s^2 Y} - \frac{1}{\beta\mathcal{N}_s^2} - \frac{\mathcal{W}u_i''(\xi)}{2\beta\mathcal{N}_s^4} - \ldots, \tag{B4}$$

and by application of the binomial theorem

$$\mathcal{N}_{\text{upper}} = \mathcal{N}_s - \frac{\mathcal{W}u_i''(\xi)}{2\beta\mathcal{N}_s}Y - \frac{\mathcal{W}}{4\mathcal{N}_s\beta^2}\left(u_i'''(\xi) - \frac{\mathcal{W}u_i''^2(\xi)}{2\mathcal{N}_s^2}\right)Y^2 - \ldots. \tag{B5}$$

By inspection, the upper solution tends to the constant $\mathcal{N}_s$ as $Y \to 0$. The lower solution is singular in this limit, and behaves as $-\mathcal{W}u_i(\xi)/\{\mathcal{N}_s^2 Y\}$. These outer solutions contain at most one singular term, so solving for $\mathcal{N}_0$ (as introduced in (39)) will be sufficient to build a global solution.

[69] Substituting for ν and ϵ in the scaled governing equation (A5), we wish to find an approximate solution to

$$-(\beta^{-1} + \mathcal{N})\frac{du_i}{dY} + u_i\frac{d\mathcal{N}}{dY} = \frac{1}{\mathcal{W}}\left(\beta^{-1} + \mathcal{N}\right)^2\left(\mathcal{N}_{\text{upper}}^2 - \mathcal{N}^2\right). \tag{B6}$$

Expanding u_i and $\mathcal{N}$ as given in equations (38) and (39), substituting for $\mathcal{N}_{\text{upper}}^2$ with (B3), and equating terms in β^0 gives

$$u_i(\xi)\frac{d\mathcal{N}_0}{dY} = \frac{1}{\mathcal{W}}\mathcal{N}_0^2\left(\mathcal{N}_s^2 - \mathcal{N}_0^2\right). \tag{B7}$$

This is a separable ordinary differential equation for $\mathcal{N}_0$. Rearranging and using partial fractions leads to the solution

$$\frac{Y}{\mathcal{W}u_i(\xi)} = -\frac{1}{\mathcal{N}_s^2\mathcal{N}_0} - \frac{1}{2\mathcal{N}_s^3}\ln(\mathcal{N}_s - \mathcal{N}_0) + \frac{1}{2\mathcal{N}_s^3}\ln(\mathcal{N}_s + \mathcal{N}_0). \tag{B8}$$

In practice, the constant of integration that is present in the general solution to (B7) has at most a small effect on $\mathcal{N}_0$, so it is typically neglected.

[70] Having obtained an implicit expression for $\mathcal{N}_0$, we check its asymptotic behavior. As $|Y| \to \infty$ in the direction of the upper steady state, the left-hand side of (B8) goes to infinity. This must be balanced by the second term on the right-hand side, so, in this limit

$$\begin{aligned} \frac{Y}{\mathcal{W}u_i(\xi)} &\approx -\frac{1}{2\mathcal{N}_s^3}\ln(\mathcal{N}_s - \mathcal{N}_0) \\ \Rightarrow \mathcal{N}_0 &\approx \mathcal{N}_s - \exp\left(-\frac{2\mathcal{N}_s^3 Y}{\mathcal{W}u_i(\xi)}\right). \end{aligned} \tag{B9}$$

Hence, $\mathcal{N}_0 \to \mathcal{N}_s$, which matches the behavior of the upper solution as $Y \to 0$. This allows us to construct a solution on the side of ξ where the outer solution is the upper steady state.

[71] As $|Y| \to \infty$ in the direction of the lower steady state, the left-hand side of (B8) goes to minus infinity. This must be balanced by the first term on the right-hand side, so, in this limit

$$\begin{aligned} \frac{Y}{\mathcal{W}u_i(\xi)} &\approx -\frac{1}{\mathcal{N}_s^2\mathcal{N}_0} \\ \Rightarrow \mathcal{N}_0 &\approx -\frac{\mathcal{W}u_i(\xi)}{\mathcal{N}_s^2 Y}. \end{aligned} \tag{B10}$$

Thus, the behavior of $\mathcal{N}_0$ in this limit matches the behavior of the lower solution as $Y \to 0$. This allows us to construct a solution on the side of ξ where the outer solution is the lower steady state.

[72] Finally, we are ready to construct the complete steady state, taking $\mathcal{N}_0$ as the inner solution. This gives

$$\mathcal{N} = \mathcal{N}_0 + \mathcal{N}_{\text{upper}} - \mathcal{N}_s, \tag{B11}$$

on the upper steady state side of ξ, and

$$\mathcal{N} = \mathcal{N}_0 + \mathcal{N}_{\text{lower}} + \frac{\mathcal{W}u_i(\xi)}{\mathcal{N}_s^2 Y}, \tag{B12}$$

on the lower steady state side of ξ. Here $\mathcal{N}_0$ is given implicitly by (B8) above.

[73] To complete the analysis, the result should be summarized in unscaled form. This is given in section 5.

Appendix C: Boundary Layer Matching Farthest From Upward Current Channel

[74] First let us note that $\xi + c = \mathcal{W}u_i(\xi)$ and that $N_s^2 = N_{\text{upper}}^2(\xi) = N_e^2(1 - \mathcal{W}u_i'(\xi)) = 0$, where primes denote differentiation with respect to y. These results are useful in what follows.

[75] We proceed according to the method outlined in section 5. Applying the scaling, noting that $u'_i(\xi) = 1/\mathcal{W}$, and using equations (24), (28), and (38) to expand $\mathcal{N}_{\text{upper}}^2$ and $\mathcal{N}_{\text{lower}}$ about ξ gives

$$\mathcal{N}_{\text{upper}}^2 = -\mathcal{W}u_i''(\xi)\beta^{2\nu-\epsilon}Y - \frac{\mathcal{W}u_i'''(\xi)\beta^{2\nu-2\epsilon}}{2}Y^2 - \ldots \tag{C1}$$

$$\mathcal{N}_{\text{lower}} = \frac{2\beta^{2\epsilon+\nu-1}u_i(\xi)}{u_i''(\xi)Y^2} + \left(\frac{2u_i'(\xi)}{u_i''(\xi)} - \frac{2u_i(\xi)u_i'''(\xi)}{3u_i''(\xi)}\right)\frac{\beta^{\epsilon+\nu-1}}{Y} - \ldots \tag{C2}$$

[76] The scaling is determined as described in Appendix A, giving $\nu = 1/5$ and $\epsilon = 2/5$. Thus, the above expansions become

$$\mathcal{N}_{\text{upper}}^2 = -\mathcal{W}u_i''(\xi)Y - \frac{\mathcal{W}u_i'''(\xi)\beta^{-2/5}}{2}Y^2 - \ldots \tag{C3}$$

$$\mathcal{N}_{\text{lower}} = \frac{2u_i(\xi)}{u_i''(\xi)Y^2} + \left(\frac{2u_i'(\xi)}{u_i''(\xi)} - \frac{2u_i(\xi)u_i'''(\xi)}{3u_i''(\xi)}\right)\frac{\beta^{-2/5}}{Y} - \ldots \tag{C4}$$

On the side of ξ on which $\mathcal{N}_{\text{upper}}$ is real, $-u_i''(\xi)Y > 0$, allowing us to sensibly take the square root of $-u_i''(\xi)Y$. Applying the binomial theorem

$$\mathcal{N}_{\text{upper}} = \sqrt{-\mathcal{W}u_i''(\xi)Y} - \frac{\beta^{-2/5}u_i'''(\xi)\sqrt{-\mathcal{W}u_i''(\xi)Y}\,Y}{4u_i''(\xi)} + \ldots \tag{C5}$$

By inspection, as $Y \to 0$, the upper solution tends to zero. The lower solution is singular in this limit, with two singular terms behaving as $1/Y$ and $1/Y^2$. These outer solutions contain at most two singular terms, so we shall solve for $\mathcal{N}_0$ and $\mathcal{N}_1$ to construct a global solution.

[77] Substituting for ν and ϵ in the scaled governing equation (A5), we wish to find an approximate solution to

$$-\left(\beta^{-4/5} + \mathcal{N}\right)\frac{du_i}{dY} + u_i\frac{d\mathcal{N}}{dY} = \frac{1}{\mathcal{W}}\left(\beta^{-4/5} + \mathcal{N}\right)^2\left(\mathcal{N}_{\text{upper}}^2 - \mathcal{N}^2\right). \tag{C6}$$

Expanding u_i and $\mathcal{N}$ as given in equations (38) and (39), substituting for $\mathcal{N}_{\text{upper}}^2$ with (C3), and equating terms in β^0 gives

$$\frac{d\mathcal{N}_0}{dY} = -\frac{\mathcal{N}_0^4}{\mathcal{W}u_i(\xi)} - \frac{u_i''(\xi)}{u_i(\xi)}\mathcal{N}_0^2 Y. \tag{C7}$$

Equating terms in $\beta^{-2/5}$ gives

$$\begin{aligned} \frac{d\mathcal{N}_1}{dY} = &-\frac{4\mathcal{N}_0^3\mathcal{N}_1}{\mathcal{W}u_i(\xi)} + \mathcal{N}_0\frac{u_i'(\xi)}{u_i(\xi)} - \left(2\mathcal{N}_0\mathcal{N}_1\frac{u_i''(\xi)}{u_i(\xi)} + \frac{d\mathcal{N}_0}{dY}\frac{u_i'(\xi)}{u_i(\xi)}\right)Y \\ &- \frac{\mathcal{N}_0^2}{2}\frac{u_i'''(\xi)}{u_i(\xi)}Y^2. \end{aligned} \tag{C8}$$

Removing $d\mathcal{N}_0/dY$ from (C8) with (C7)

$$\frac{d\mathcal{N}_1}{dY} = \frac{\mathcal{N}_0}{u_i(\xi)}\left(u_i'(\xi) - \frac{4\mathcal{N}_0^2\mathcal{N}_1}{\mathcal{W}}\right) + \frac{\mathcal{N}_0}{u_i(\xi)}\left(\frac{\mathcal{N}_0^3 u_i'(\xi)}{\mathcal{W}u_i(\xi)} - 2\mathcal{N}_1 u_i''(\xi)\right)Y + \frac{\mathcal{N}_0^2}{u_i(\xi)}\left(\frac{u_i'(\xi)u_i''(\xi)}{u_i(\xi)} - \frac{u_i'''(\xi)}{2}\right)Y^2. \tag{C9}$$

[78] We now use the above equations to obtain the asymptotic behavior of $\mathcal{N}_0$ and $\mathcal{N}_1$. As $|Y| \to \infty$ in the direction of the upper steady state, the second term on the right-hand side of (C7) goes to sign$(u_i)\infty$. This is balanced by the first term on the right-hand side, so, in this limit

$$\frac{\mathcal{N}_0^4}{\mathcal{W}u_i(\xi)} \approx -\frac{u_i''(\xi)}{u_i(\xi)}\mathcal{N}_0^2 Y \Rightarrow \mathcal{N}_0 \approx \sqrt{-\mathcal{W}u_i''(\xi)Y}. \tag{C10}$$

As $|Y| \to \infty$ in the direction of the lower steady state, the second term on the right-hand side of (C7) goes to $-$sign $(u_i)\infty$. This is balanced by the term on the left-hand side, giving

$$\frac{d\mathcal{N}_0}{dY} \approx -\frac{u_i''(\xi)}{u_i(\xi)}\mathcal{N}_0^2 Y \Rightarrow -\int\frac{d\mathcal{N}_0}{\mathcal{N}_0^2} \approx \frac{u_i''(\xi)}{u_i(\xi)}\int Y dY \Rightarrow \mathcal{N}_0 \approx \frac{2u_i(\xi)}{u_i''(\xi)Y}. \tag{C11}$$

[79] Next we consider the asymptotic behavior of $\mathcal{N}_1$. As $|Y| \to \infty$ in the direction of the upper steady state, we can use (C10) to substitute for $\mathcal{N}_0$ in (C9). After rearranging, this gives

$$\frac{d\mathcal{N}_1}{dY} \approx \frac{u_i'(\xi)}{u_i(\xi)}\sqrt{-\mathcal{W}u_i''(\xi)Y} + \frac{2\mathcal{N}_1 u_i''(\xi)}{u_i(\xi)}\sqrt{-\mathcal{W}u_i''(\xi)Y}Y + \frac{\mathcal{W}u_i''(\xi)u_i'''(\xi)}{2u_i(\xi)}Y^3. \tag{C12}$$

In this limit, the term in Y^3 is balanced by the term in $\sqrt{-\mathcal{W}u_i''(\xi)Y}Y$, so

$$\frac{2\mathcal{N}_1 u_i''(\xi)}{u_i(\xi)}\sqrt{-\mathcal{W}u_i''(\xi)Y}Y \approx -\frac{\mathcal{W}u_i''(\xi)u_i'''(\xi)}{2u_i(\xi)}Y^3 \Rightarrow \mathcal{N}_1 \approx -\frac{u_i'''(\xi)\sqrt{-\mathcal{W}u_i''(\xi)Y}Y}{4u_i''(\xi)}. \tag{C13}$$

[80] As $|Y| \to \infty$ in the direction of the lower steady state, we can use (C11) to substitute for $\mathcal{N}_0$ in (C9). After rearranging, this gives

$$\frac{d\mathcal{N}_1}{dY} \approx -\frac{4\mathcal{N}}{Y} + \frac{6u_i'(\xi)}{u_i''(\xi)Y^2} - \frac{2u_i(\xi)u_i'''(\xi)}{u_i'''^2(\xi)Y^2} - \frac{32\mathcal{N}_1 u_i^2(\xi)u_i'(\xi)}{u_i''(\xi)Y^6} + \frac{16u_i^2(\xi)u_i'(\xi)}{u_i''^4(\xi)Y^7}. \tag{C14}$$

In this limit, terms in Y^{-6} and Y^{-7} may be neglected, so we solve the following first-order ordinary differential equation:

$$\frac{d\mathcal{N}_1}{dY} + \frac{4}{Y}\mathcal{N}_1 \approx \left(\frac{6u_i'(\xi)}{u_i''(\xi)} - \frac{2u_i(\xi)u_i'''(\xi)}{u_i''^2(\xi)}\right)\frac{1}{Y^2} \Rightarrow \mathcal{N}_1 \approx \left(\frac{2u_i'(\xi)}{u_i''(\xi)} - \frac{2u_i(\xi)u_i'''(\xi)}{3u_i''^2(\xi)}\right)\frac{1}{Y}. \tag{C15}$$

[81] From these asymptotic solutions, we see that

$$\mathcal{N}_{\text{inner}} = \mathcal{N}_0 + \beta^{-2/5}\mathcal{N}_1$$

picks up the behavior of the outer solutions in the appropriate limits. This allows us to construct the complete steady state as

$$\mathcal{N} = \mathcal{N}_0 + \beta^{-2/5}\mathcal{N}_1 + \mathcal{N}_{\text{upper}} - \sqrt{-\mathcal{W}u_i''(\xi)Y} + \frac{\beta^{-2/5}u_i'''(\xi)\sqrt{-\mathcal{W}u_i''(\xi)Y}Y}{4u_i''(\xi)} \tag{C16}$$

on the upper steady state side of ξ, and

$$\mathcal{N} = \mathcal{N}_0 + \beta^{-2/5}\mathcal{N}_1 + \mathcal{N}_{\text{lower}} - \frac{2u_i(\xi)}{u_i''(\xi)Y^2} + \left(\frac{2u_i'(\xi)}{u_i''(\xi)} - \frac{2u_i(\xi)u_i'''(\xi)}{3u_i''(\xi)}\right)\frac{\beta^{-2/5}}{Y}, \tag{C17}$$

on the lower steady state side of ξ. Here $\mathcal{N}_0$ and $\mathcal{N}_1$ are the solutions to ordinary differential equations (C7) and (C9), respectively.

[82] To complete the analysis, the result should be summarized in unscaled form. This is given in section 5.

[83] **Acknowledgments.** A.J.B.R. is supported by an STFC studentship. A.N.W. is grateful to the International Space Science Institute (Switzerland) for funding the program through which this work was completed.

[84] Amitava Bhattacharjee thanks Michael Ruderman and another reviewer for their assistance in evaluating this paper.

References

Aikio, A. T., T. Lakkala, A. Kozlovsky, and P. J. S. Williams (2002), Electric fields and currents of stable drifting auroral arcs in the evening sector, *J. Geophys. Res.*, *107*(A12), 1424, doi:10.1029/2001JA009172.

Aikio, A., et al. (2004), Temporal evolution of two auroral arcs as measured by the Cluster satellite and coordinated ground-based instruments, *Ann. Geophys.*, *22*, 4089–4101.

Blixt, E. M., and A. Brekke (1996), A model of currents and electric fields in a discrete auroral arc, *Geophys. Res. Lett.*, *23*, 2553–2556, doi:10.1029/96GL02378.

Cran-McGreehin, A. P., A. N. Wright, and A. W. Hood (2007), Ionospheric depletion in auroral downward currents, *J. Geophys. Res.*, *112*, A10309, doi:10.1029/2007JA012350.

Doe, R. A., J. F. Vickrey, and M. Mendillo (1995), Electrodynamic model for the formation of auroral ionospheric cavities, *J. Geophys. Res.*, *100*, 9683–9696, doi:10.1029/95JA00001.

Karlsson, T., and G. T. Marklund (1999), Results from the DC electric field experiment on the Freja satellite, *Adv. Space Res.*, *23*, 1657–1665, doi:10.1016/S0273-1177(99)00375-0.

Marklund, G. T., et al. (2001), Temporal evolution of the electric field accelerating electrons away from the auroral ionosphere, *Nature*, *414*, 724–727.

Mishin, E. V., W. J. Burke, C. Y. Huang, and F. J. Rich (2003), Electromagnetic wave structures within subauroral polarization streams, *J. Geophys. Res.*, *108*,(A8), 1309, doi:10.1029/2002JA009793.

Paschmann, G., S. Haaland, and R. Treumann (2002), *Auroral Plasma Physics*, *Space Sci. Rev.*, vol. 103, Springer, Berlin, doi:10.1023/A:1023088315789.

Streltsov, A. V., and W. Lotko (2004), Multiscale electrodynamics of the ionosphere-magnetosphere system, *J. Geophys. Res.*, *109*, A09214, doi:10.1029/2004JA010457.

Streltsov, A. V., and W. Lotko (2005), Ultra-low-frequency electrodynamics of the magnetosphere-ionosphere interaction, *J. Geophys. Res.*, *110*, A08203, doi:10.1029/2004JA010764.

Streltsov, A. V., and W. Lotko (2008), Coupling between density structures, electromagnetic waves and ionospheric feedback in the auroral zone, *J. Geophys. Res.*, *113*, A05212, doi:10.1029/2007JA012594.

Wei, C. Q., J. C. Samson, R. Rankin, and P. Frycz (1994), Electron inertial effects on geomagnetic field line resonances, *J. Geophys. Res.*, *99*, 11,265–11,276, doi:10.1029/94JA00582.

Wright, A. N. (2005), Energy sources of field-aligned currents: Auroral electron energization, *J. Geophys. Res.*, *110*, A10S08, doi:10.1029/2004JA010609.

Wright, A. N., W. Allan, M. S. Ruderman, and R. C. Elphic (2002), The dynamics of current carriers in standing Alfvén waves: Parallel electric fields in the auroral acceleration region, *J. Geophys. Res.*, *107*(A7), 1120, doi:10.1029/2001JA900168.

Wright, A. N., C. J. Owen, C. C. Chaston, and M. W. Dunlop (2008), Downward current electron beam observed by Cluster and FAST, *J. Geophys. Res.*, *113*, A06202, doi:10.1029/2007JA012643.

A. W. Hood, A. J. B. Russell, and A. N. Wright, School of Mathematics and Statistics, University of St. Andrews, North Haugh, St. Andrews, Fife KY16 9SS, Scotland, UK. (alexr@mcs.st-andrews.ac.uk)